Stochastic Aerospace Systems Practical

AE4304P

Pedro Tallón Marrón

TU Delft

Stochastic Aerospace Systems Practical

by

Pedro Tallón Marrón

Student Name	Student Number
Pedro Tallón Marrón	5342120

Instructor: dr. ir. E.J.J. Smeur
Faculty: Faculty of Aerospace Engineering, Delft

Style: TU Delft Report Style, with modifications by Daan Zwaneveld

TU Delft

Contents

1

Introduction

Aircraft operating in real-world environments are continuously subjected to stochastic atmospheric disturbances, such as turbulence, which influence their dynamic behaviour. Understanding how an aircraft responds to these disturbances is essential to ensure stability, performance, and passenger comfort. This practical assignment aims to analyse the stochastic response of a Cessna Ce500 Citation I subjected to asymmetrical atmospheric turbulence, modelled using the Dryden spectrum, under cruise conditions.

The study focusses on applying time and frequency domain analysis techniques to evaluate aircraft stability and response characteristics in turbulent conditions. The assignment involves modelling two different aircraft configurations: (1) a full set of equations of motion and (2) a simplified model approximating the Dutch roll mode, which assumes no roll motion and constant course. Furthermore, a stability analysis is conducted to determine whether the aircraft requires a roll-damping control system to maintain stability.

Following stability analysis, time-domain simulations are performed to observe the responses of the aircraft state to turbulence. These simulations provide insight into the relationship between lateral turbulence and key states, such as lateral acceleration. Additionally, spectral analysis is conducted to compute the Power Spectral Density (PSD) of the aircraft states, using both analytical and experimental methods. The accuracy and limitations of these methods are compared to assess their effectiveness in characterising the frequency domain behaviour of the system.

Finally, the variance of the aircraft states is estimated using the different approaches previously used to perform the PSD computations. These variance estimates help quantify the impact of turbulence on aircraft behaviour and highlight differences between the two models under study.

Through this assignment, key principles of stochastic aerospace systems are reinforced, demonstrating the applicability of spectral and statistical methods in aircraft response analysis. The results contribute to a deeper understanding of how turbulence affects aircraft dynamics and how different computational techniques can be leveraged to analyse stochastic processes.

2

Preliminary Calculations

2.1. Model Definition

As exposed previously in the introduction, in this project the turbulence analysis is performed to two different models: a first full lateral model with the complete set of equations of motion and a second simplified model approximating the Dutch Roll.

The full lateral model has been extracted directly from [3] and modified accordingly with the specifications of the assignment. Since in this project the analysis is performed to only lateral turbulence, the states related to the longitudinal, $\begin{bmatrix}\hat{u}_g^* & \hat{u}_g\end{bmatrix}$, and vertical turbulence, $\begin{bmatrix}\alpha_g^* & \alpha_g\end{bmatrix}$, and the white noise inputs driving the turbulence generating filters, w_1 and w_3, have been obviated. With this in mind, the following modified state-space matrices were obtained:

$$\mathbf{A} = \begin{bmatrix} y_\beta & y_\phi & y_p & y_r & y_{\beta_g} & 0 \\ 0 & 0 & \frac{2V}{b} & 0 & 0 & 0 \\ l_\beta & 0 & l_p & l_r & l_{\beta_g} & 0 \\ n_\beta & 0 & n_p & n_r & n_{\beta_g} & 0 \\ 0 & 0 & 0 & 0 & 0 & 1 \\ 0 & 0 & 0 & 0 & -\left(\frac{V}{L_g}\right)^2 & -\frac{2V}{L_g} \end{bmatrix} \tag{2.1}$$

and

$$\mathbf{B} = \begin{bmatrix} 0 & y_{\delta_r} & 0 \\ 0 & 0 & 0 \\ l_{\delta_a} & l_{\delta_r} & 0 \\ n_{\delta_a} & n_{\delta_r} & 0 \\ 0 & 0 & \sigma_{\beta_g}\sqrt{\frac{3V}{L_g}} \\ 0 & 0 & (1-2\sqrt{3})\sigma_{\beta_g}\sqrt{\left(\frac{V}{L_g}\right)^3} \end{bmatrix}. \tag{2.2}$$

It should be noted that in the previous definition of the state and input matrices, the abbreviated form of the coefficients has been included to accommodate correctly the definitions. The definitions of all the included parameters are found in Appendix A in Table A.1 and Table A.2.

Taking all the previous into consideration, the asymmetrical state-space representation final result is,

$$\begin{bmatrix} \dot{\beta} \\ \dot{\phi} \\ \frac{\dot{p}b}{2V} \\ \frac{\dot{r}b}{2V} \\ \dot{\beta}_g \\ \dot{\beta}_g^* \end{bmatrix} = \begin{bmatrix} y_\beta & y_\phi & y_p & y_r & y_{\beta_g} & 0 \\ 0 & 0 & \frac{2V}{b} & 0 & 0 & 0 \\ l_\beta & 0 & l_p & l_r & l_{\beta_g} & 0 \\ n_\beta & 0 & n_p & n_r & n_{\beta_g} & 0 \\ 0 & 0 & 0 & 0 & 0 & 1 \\ 0 & 0 & 0 & 0 & -\left(\frac{V}{L_g}\right)^2 & -\frac{2V}{L_g} \end{bmatrix} \cdot \begin{bmatrix} \beta \\ \phi \\ \frac{pb}{2V} \\ \frac{rb}{2V} \\ \beta_g \\ \beta_g^* \end{bmatrix} + \begin{bmatrix} 0 & y_{\delta_r} & 0 \\ 0 & 0 & 0 \\ l_{\delta_a} & l_{\delta_r} & 0 \\ n_{\delta_a} & n_{\delta_r} & 0 \\ 0 & 0 & \sigma_{\beta_g}\sqrt{\frac{3V}{L_g}} \\ 0 & 0 & (1-2\sqrt{3})\sigma_{\beta_g}\sqrt{\left(\frac{V}{L_g}\right)^3} \end{bmatrix} \cdot \begin{bmatrix} \delta_a \\ \delta_r \\ w_2 \end{bmatrix}. \tag{2.3}$$

The second model used in this exercise is a simplification of the equations of motion that approximates the Dutch roll. In this way, the first step to perform will be to present the asymmetric equations of motion of the aircraft,

$$\begin{bmatrix} C_{Y_\beta} - 2\mu_b D_b & C_L & C_{Y_p} & C_{Y_r} - 4\mu_b \\ 0 & -\frac{1}{2}D_b & 1 & 0 \\ C_{l_\beta} & 0 & C_{l_p} - 4\mu_b K_X^2 D_b & C_{l_r} + 4\mu_b K_{XZ} D_b \\ C_{n_\beta} & 0 & C_{n_p} + 4\mu_b K_{XZ} D_b & C_{n_r} - 4\mu_b K_Z^2 D_b \end{bmatrix} \cdot \begin{bmatrix} \beta \\ \phi \\ \frac{pb}{2V} \\ \frac{rb}{2V} \end{bmatrix} = - \begin{bmatrix} 0 & C_{Y_{\delta_r}} & C_{Y_\beta} \\ 0 & 0 & 0 \\ C_{l_{\delta_a}} & C_{l_{\delta_r}} & C_{l_\beta} \\ C_{n_{\delta_a}} & C_{n_{\delta_r}} & C_{n_\beta} \end{bmatrix} \cdot \begin{bmatrix} \delta_a \\ \delta_r \\ \beta_g \end{bmatrix}, \tag{2.4}$$

where $D_b = \frac{b}{V}\frac{d}{dt}$.

The first simplification, is that the rolling component is discarded in the Dutch roll motion. If ϕ and p are set to zero, their respective columns on the equations of motion disappear and the moment equation of the roll goes away, since it needs to stay in balance [1]. With this, only the aerodynamic force Y and moment N equations remain. The result of this simplification is,

$$\begin{bmatrix} C_{Y_\beta} - 2\mu_b D_b & C_{Y_r} - 4\mu_b \\ C_{n_\beta} & C_{n_r} - 4\mu_b K_Z^2 D_b \end{bmatrix} \cdot \begin{bmatrix} \beta \\ \frac{rb}{2V} \end{bmatrix} = - \begin{bmatrix} 0 & C_{Y_{\delta_r}} & C_{Y_\beta} \\ C_{n_{\delta_a}} & C_{n_{\delta_r}} & C_{n_\beta} \end{bmatrix} \cdot \begin{bmatrix} \delta_a \\ \delta_r \\ \beta_g \end{bmatrix}. \tag{2.5}$$

The second simplification to perform is more restrictive than the previous, and it is only considering the yawing rotation. In other words, the movement of the aircraft's centre of gravity is a straight line during the oscillation, making the course angle $\mathcal{X}$ constant, where $\mathcal{X} = \beta + \psi = 0$, or $\beta = -\psi$. This assumption, makes the equation Y superfluous, but introduces a new relation,

$$\dot{\beta} = -\dot{\psi} = -r = -\frac{rb}{2V} \cdot \frac{2V}{b} \Rightarrow \frac{D_b}{2}\beta + \frac{rb}{2V} = 0. \tag{2.6}$$

Introducing this equation, as the first lateral equation of motion, and retaining the moment N equation, the following system is obtained,

$$\begin{bmatrix} \frac{D_b}{2} & 1 \\ C_{n_\beta} & C_{n_r} - 4\mu_b K_Z^2 D_b \end{bmatrix} \cdot \begin{bmatrix} \beta \\ \frac{rb}{2V} \end{bmatrix} = - \begin{bmatrix} 0 & 0 & 0 \\ C_{n_{\delta_a}} & C_{n_{\delta_r}} & C_{n_\beta} \end{bmatrix} \cdot \begin{bmatrix} \delta_a \\ \delta_r \\ \beta_g \end{bmatrix}. \tag{2.7}$$

The state-space form can be extracted by rearranging Equation 2.7. To start off, the terms with the differential operator D_b are kept on the left-hand side of the equation, while the rest of the terms are shifted to the right-hand side. Moreover, D_b is replaced by $\frac{b}{V}\frac{d}{dt}$. This leads to,

$$\begin{bmatrix} \frac{1}{2}\frac{b}{V}\frac{d}{dt} & 0 \\ 0 & -4\mu_b K_Z^2 \frac{b}{V}\frac{d}{dt} \end{bmatrix} \cdot \begin{bmatrix} \beta \\ \frac{rb}{2V} \end{bmatrix} = - \begin{bmatrix} 0 & 1 \\ C_{n_\beta} & C_{n_r} \end{bmatrix} \cdot \begin{bmatrix} \beta \\ \frac{rb}{2V} \end{bmatrix} - \begin{bmatrix} 0 & 0 \\ C_{n_{\delta_r}} & C_{n_\beta} \end{bmatrix} \cdot \begin{bmatrix} \delta_r \\ \beta_g \end{bmatrix}. \tag{2.8}$$

By extracting the temporal differentials and moving them to the state space vector,

$$\begin{bmatrix} \frac{1}{2}\frac{b}{V} & 0 \\ 0 & -4\mu_b K_Z^2 \frac{b}{V} \end{bmatrix} \cdot \begin{bmatrix} \dot{\beta} \\ \frac{\dot{r}b}{2V} \end{bmatrix} = - \begin{bmatrix} 0 & 1 \\ C_{n_\beta} & C_{n_r} \end{bmatrix} \cdot \begin{bmatrix} \beta \\ \frac{rb}{2V} \end{bmatrix} - \begin{bmatrix} 0 & 0 & 0 \\ C_{n_{\delta_a}} & C_{n_{\delta_r}} & C_{n_\beta} \end{bmatrix} \cdot \begin{bmatrix} \delta_a \\ \delta_r \\ \beta_g \end{bmatrix}. \tag{2.9}$$

Finally, the matrix multiplying the state vector derivatives is inverted and multiplied to the right-hand side terms. In this case, since it is a 2×2 diagonal matrix, its inverse is another diagonal matrix with elements equal to the reciprocals of the original diagonal elements. This results in the following expression,

$$\begin{bmatrix} \dot{\beta} \\ \frac{\dot{r}b}{2V} \end{bmatrix} = \begin{bmatrix} 0 & -\frac{2V}{b} \\ \frac{C_{n_\beta}}{4\mu_b K_Z^2 \frac{b}{V}} & \frac{C_{n_r}}{4\mu_b K_Z^2 \frac{b}{V}} \end{bmatrix} \cdot \begin{bmatrix} \beta \\ \frac{rb}{2V} \end{bmatrix} + \begin{bmatrix} 0 & 0 & 0 \\ \frac{C_{n_{\delta_a}}}{4\mu_b K_Z^2 \frac{b}{V}} & \frac{C_{n_{\delta_r}}}{4\mu_b K_Z^2 \frac{b}{V}} & \frac{C_{n_\beta}}{4\mu_b K_Z^2 \frac{b}{V}} \end{bmatrix} \cdot \begin{bmatrix} \delta_a \\ \delta_r \\ \beta_g \end{bmatrix}. \tag{2.10}$$

As performed previously, an abbreviated form of the simplified state-space is defined for an easier handling. The state-space of Equation 2.12 in compressed form is,

$$\begin{bmatrix} \dot{\beta} \\ \frac{\dot{r}b}{2V} \end{bmatrix} = \begin{bmatrix} 0 & \tilde{y}_r \\ \tilde{n}_\beta & \tilde{n}_r \end{bmatrix} \cdot \begin{bmatrix} \beta \\ \frac{rb}{2V} \end{bmatrix} + \begin{bmatrix} 0 & 0 & 0 \\ \tilde{n}_{\delta_a} & \tilde{n}_{\delta_r} & \tilde{n}_{\beta_g} \end{bmatrix} \cdot \begin{bmatrix} \delta_a \\ \delta_r \\ \beta_g \end{bmatrix}. \tag{2.11}$$

With the defined asymmetrical simplified state space, the next step is the addition of the turbulence filters as defined in [3] and included in Equation 2.3. Including the relevant inputs for lateral turbulence, the simplified model state-space representation used is,

$$\begin{bmatrix} \dot{\beta} \\ \frac{\dot{r}b}{2V} \\ \dot{\beta}_g \\ \dot{\beta}_g^* \end{bmatrix} = \begin{bmatrix} 0 & \tilde{y}_r & 0 & 0 \\ \tilde{n}_\beta & \tilde{n}_r & \tilde{n}_{\beta_g} & 0 \\ 0 & 0 & 0 & 1 \\ 0 & 0 & -\left(\frac{V}{L_g}\right)^2 & -\frac{2V}{L_g} \end{bmatrix} \cdot \begin{bmatrix} \beta \\ \frac{rb}{2V} \\ \beta_g \\ \beta_g^* \end{bmatrix} + \begin{bmatrix} 0 & 0 & 0 \\ \tilde{n}_{\delta_a} & \tilde{n}_{\delta_r} & 0 \\ 0 & 0 & \sigma_{\beta_g}\sqrt{\frac{3V}{L_g}} \\ 0 & 0 & (1-2\sqrt{3})\sigma_{\beta_g}\sqrt{\left(\frac{V}{L_g}\right)^3} \end{bmatrix} \cdot \begin{bmatrix} \delta_a \\ \delta_r \\ w_2 \end{bmatrix}. \tag{2.12}$$

2.2. Stability Analysis

After deriving the models for this exercise, a stability analysis is performed to ensure that the aircraft remains stable in the specified flight conditions for both models. With this in mind, the first step is to extract the poles of both models, or which is the same, the eigenvalues of the state matrices. The results are included in Table 2.1.

Poles	
Full model	**Simplified model**
$-0.3028 + 3.7423i$	$-0.2774 + 3.8109i$
$-0.3028 - 3.7423i$	$-0.2774 - 3.8109i$
$-3.7836 + 0.0000i$	$-1.2127 + 0.0000i$
$0.0037 + 0.0000i$	$-1.2127 + 0.0000i$
$-1.2127 + 0.0000i$	
$-1.2127 + 0.0000i$	

Table 2.1: Eigenvalues of the full and simplified model.

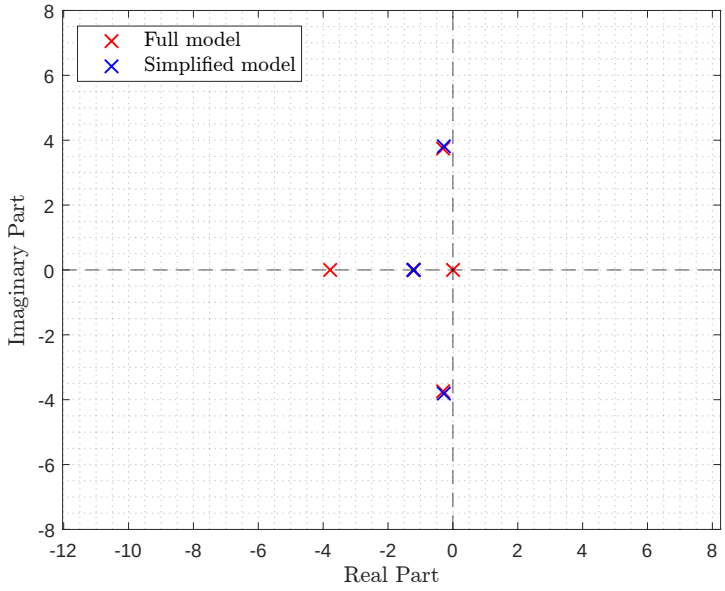

Figure 2.1: Representation of the poles of the full and simplified model.

From Table 2.1, several conclusions can be drawn. To start off, it can be seen that in both cases a real pole is repeated, -1.2127, which is related to the introduction of the gust filter. Furthermore, it is clear that the full model is unstable since it has one right-half-plane (RHP) pole, related to the Spiral eigenmotion.

To stabilize the system, a roll damper of the form

$$\delta_a = K_\phi \cdot \phi \ + K_p \cdot p, \tag{2.13}$$

needs to be designed. This type of controller would not affect the simplified model since one of the simplifications is that no roll is considered. However, since the simplified model is already stable, such a controller would not be necessary.

To add this control law in the model, the Equation 2.13 has been substituted as input in Equation 2.3 affecting the L and N moments equations, since they are the only equations with non-zero terms in the δ_a input. This equations result in,

$$\frac{\dot{p}b}{2V} = l_\beta \cdot \beta + l_p \cdot \frac{pb}{2V} + l_r \cdot \frac{rb}{2V} + l_{\beta_g} \cdot \beta_g + l_{\delta_r} \cdot \delta_r + l_{\delta_a} \cdot (K_\phi \cdot \phi \ + K_p \cdot p)\,, \tag{2.14}$$

$$\frac{\dot{r}b}{2V} = n_\beta \cdot \beta + n_p \cdot \frac{pb}{2V} + n_r \cdot \frac{rb}{2V} + n_{\beta_g} \cdot \beta_g + n_{\delta_r} \cdot \delta_r + n_{\delta_a} \cdot (K_\phi \cdot \phi \ + K_p \cdot p)\,, \tag{2.15}$$

which after rearranging, a new state matrix can be defined, named in this exercise the controlled state matrix,

$$\mathbf{A}_c = \begin{bmatrix} y_\beta & y_\phi & y_p & y_r & y_{\beta_g} & 0 \\ 0 & 0 & \frac{2V}{b} & 0 & 0 & 0 \\ l_\beta & l_{\delta_a} \cdot K_\phi & l_p + l_{\delta_a} \cdot K_p \frac{2V}{b} & l_r & l_{\beta_g} & 0 \\ n_\beta & n_{\delta_a} \cdot K_\phi & n_p + n_{\delta_a} \cdot K_p \frac{2V}{b} & n_r & n_{\beta_g} & 0 \\ 0 & 0 & 0 & 0 & 0 & 1 \\ 0 & 0 & 0 & 0 & -\left(\frac{V}{L_g}\right)^2 & -\frac{2V}{L_g} \end{bmatrix}. \tag{2.16}$$

With this new state matrix, the Level 1 flying qualities of the MIL-F-8785C standard has been selected, for the cruise condition, as a baseline to ensure that the aircraft had sufficient handling qualities. The Dutch Roll minimum values for cruise conditions, Category B, are $\omega_d = 0.4$, $\zeta_d = 0.08$ and $\omega_d \zeta_d = 0.15$[1]. Using this values as baseline, the selected constants of the controller are included in Table 2.2.

[1]The values have been extracted from Table A.3, which is in Appendix A.

Roll-damper	
$K_\phi = 0.1$	$K_p = 0.1$

Table 2.2: Selected roll-damper parameters.

Using the previously mentioned control law, the resulting eigenvalues of the full model, as well as frequency and damping ratio, are included in Table 2.3.

Uncontrolled Poles	**Controlled Poles**	ω_d [rad/s]	ζ_d [-]	$\omega_d\zeta_d$ [rad/s]
$-3.7836 + 0.0000i$	$-7.8189 + 0i$	7.8189	1	7.8189
$-0.3028 + 3.7423i$	$-0.34838 + 3.8083i$	3.8242	0.091097	0.34838
$-0.3028 - 3.7423i$	$-0.34838 - 3.8083i$	3.8242	0.091097	0.34838
$0.0037 + 0.0000i$	$-0.60225 + 0i$	0.60225	1	0.60225
$-1.2127 + 0.0000i$	$-1.2127 + 0i$	1.2127	1	1.2127
$-1.2127 + 0.0000i$	$-1.2127 + 0i$	1.2127	1	1.2127

Table 2.3: Comparison of the poles of the controlled and uncontrolled full model.

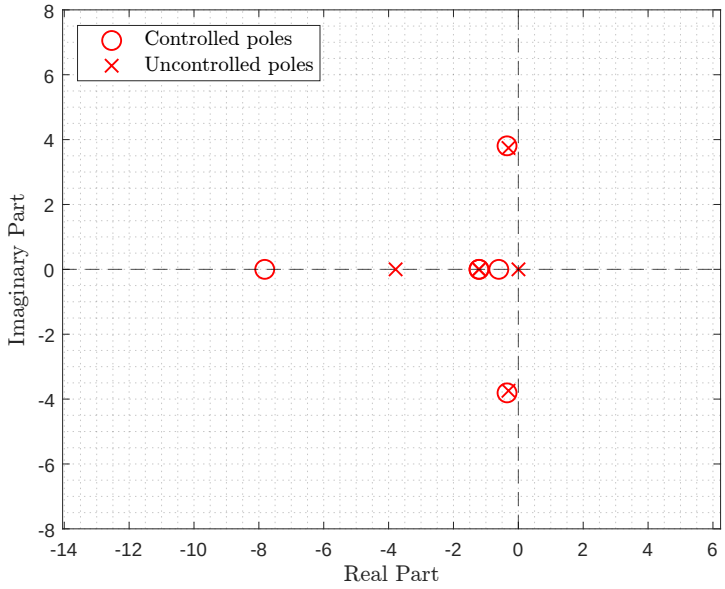

Figure 2.2: Representation of the poles of the controled and uncontrolled full model.

With respect to spiral motion, MIL-F-8785C specifies minimum requirements for the case of a divergent motion [2]. Since the motion is stable in the controlled case, it complies with these requirements. Moreover, regarding the simplified model, since the control law does not introduce any changes, the poles remain unchanged as exposed in Table 2.4. Consequently, the poles of both controlled models are included in Figure 2.3.

Poles	ω_d [rad/s]	ζ_d [-]	$\omega_d\zeta_d$ [rad/s]
$-0.27742 + 3.8109i$	3.821	0.072605	0.27742
$-0.27742 - 3.8109i$	3.821	0.072605	0.27742
$-1.2127 + 0i$	1.2127	1	1.2127
$-1.2127 + 0i$	1.2127	1	1.2127

Table 2.4: Poles and characteristic properties of the simplified model.

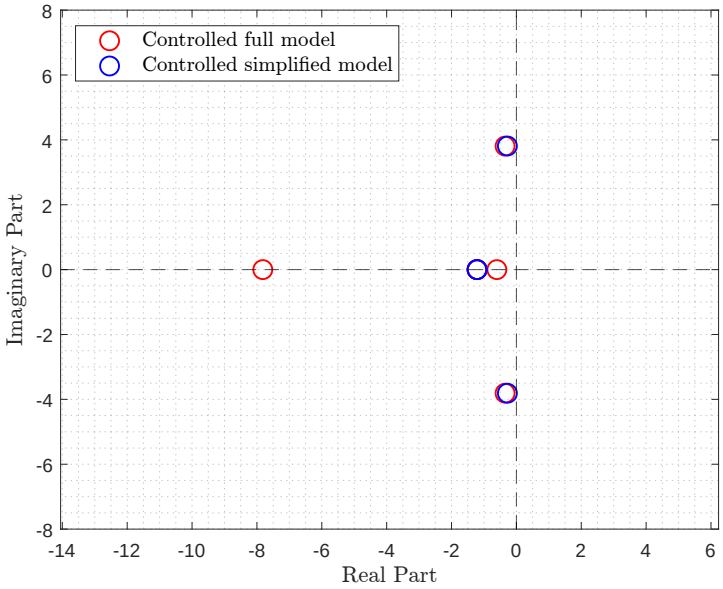

Figure 2.3: Representation of the poles of the controlled full and simplified model.

Based on the previous analysis, the controlled system can be considered stable, and further analysis will be conducted in the following chapters.

3

Time-Domain Simulations

In this chapter, the previously defined models are used to extract the temporal evolutions of the aircraft state variables under lateral turbulence. These time domain responses are simulated using the noise input w_2 exposed in Equation 2.3 and Equation 2.12.

In addition to the state variables, the response of an additional variable has been extracted, the lateral acceleration a_y. This variable is defined as,

$$a_y = V \cdot (\dot{\psi} + \dot{\beta}) = V \cdot (r + \dot{\beta}). \tag{3.1}$$

In this way, to extract the desired responses, $\mathbf{C}$ must be correctly defined. To extract the time responses of the relevant states, the aircraft lateral variables, the first four rows are an identity matrix. With respect to the lateral acceleration response, the last row of the matrix has been defined as the first row of $\mathbf{A}$ times V plus the contribution of the term of the yaw rate times V. This has been extracted from Equation 3.1. With this, the definition of $\mathbf{C}$ and $\tilde{\mathbf{C}}$, for the full and simplified model respectively, used is,

$$\mathbf{C} = \begin{bmatrix} 1 & 0 & 0 & 0 & 0 & 0 \\ 0 & 1 & 0 & 0 & 0 & 0 \\ 0 & 0 & 1 & 0 & 0 & 0 \\ 0 & 0 & 0 & 1 & 0 & 0 \\ y_\beta \cdot V & y_\phi \cdot V & y_p \cdot V & y_r \cdot V + \frac{2V^2}{b} & y_{\beta_g} \cdot V & 0 \end{bmatrix}, \tag{3.2}$$

$$\tilde{\mathbf{C}} = \begin{bmatrix} 1 & 0 & 0 & 0 \\ 0 & 1 & 0 & 0 \\ 0 & -\frac{2V}{b} \cdot V + \frac{2V^2}{b} & 0 & 0 \end{bmatrix} = \begin{bmatrix} 1 & 0 & 0 & 0 \\ 0 & 1 & 0 & 0 \\ 0 & 0 & 0 & 0 \end{bmatrix}. \tag{3.3}$$

With respect to the definition of $\mathbf{D}$, a similar approach has been taken as in the case of $\mathbf{C}$. For the first rows, since the states are extracted as outputs, these rows consist of zeros. In the last row, since the lateral acceleration depends on $\dot{\beta}$, the inputs should be considered. For the complete model, it is true that the only non-zero coefficient is the one related to δ_r. However, since the only input in the time-domain simulations is the noise w_2, this has no effect.

Given this, the definitions of $\mathbf{D}$ and $\tilde{\mathbf{D}}$, for the full and simplified models, respectively, are:

$$\mathbf{D} = \begin{bmatrix} 0 & 0 & 0 \\ 0 & 0 & 0 \\ 0 & 0 & 0 \\ 0 & 0 & 0 \\ 0 & y_{\delta_r} \cdot V & 0 \end{bmatrix}, \tag{3.4}$$

$$\tilde{\mathbf{D}} = \begin{bmatrix} 0 & 0 & 0 \\ 0 & 0 & 0 \\ 0 & 0 & 0 \end{bmatrix}. \tag{3.5}$$

From the previous equations, a noticeable aspect can be observed in the last row of $\tilde{\mathbf{C}}$ and $\tilde{\mathbf{D}}$. All terms in this row are zero, indicating that for any lateral noise input to the system, no lateral acceleration is measured. This result is expected, as the definition of $\beta = -\psi$ implies a constant course at all times. In other words, the lateral force equation Y is balanced and, thus, no lateral acceleration should be experienced. Taking into account all previous calculations, the simulation results for the full and simplified model are included in Figure 3.1.

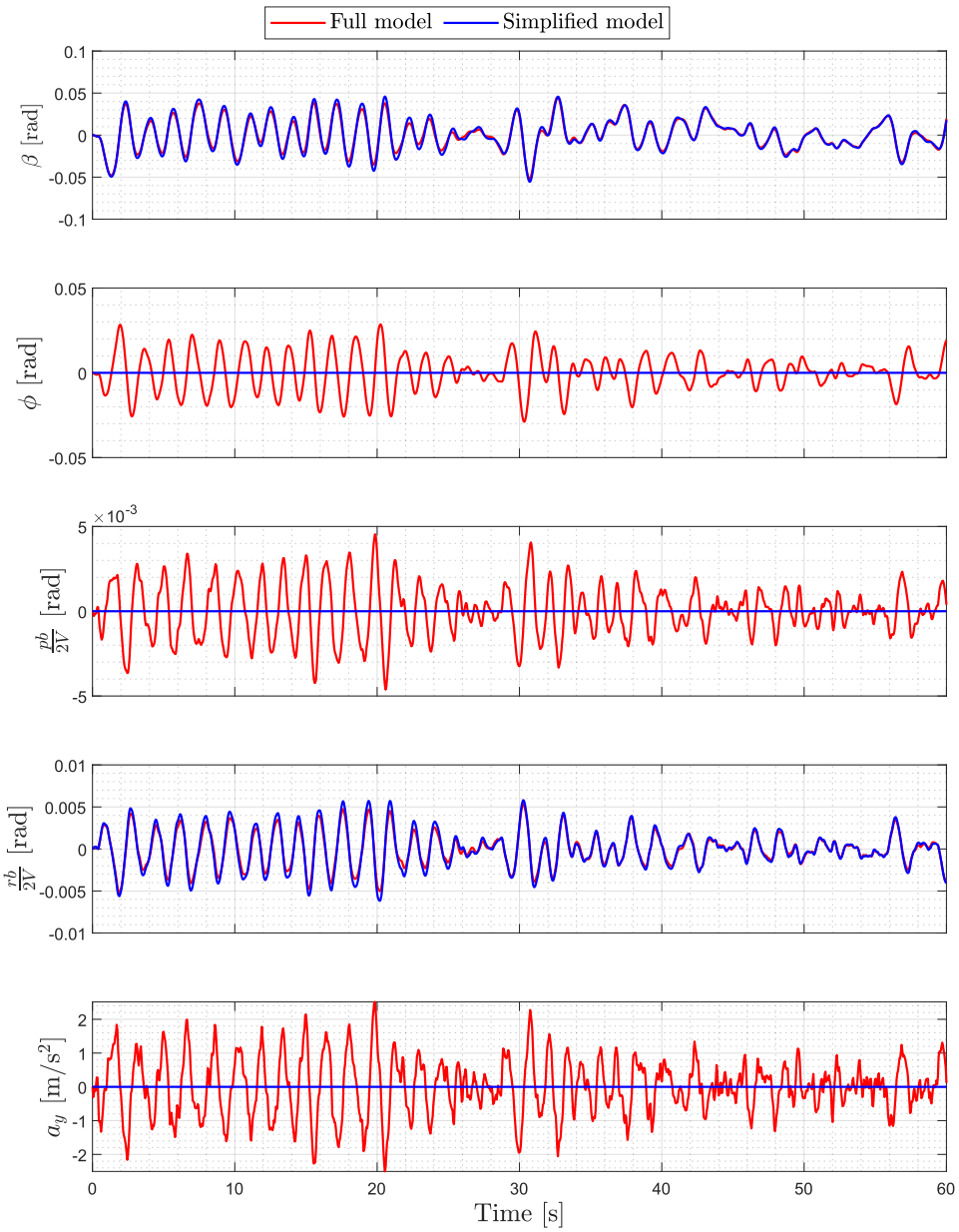

Figure 3.1: Time domain representation of the states and lateral acceleration a_y, for both complete and simplified aircraft models.

As discussed previously, in Figure 3.1 it can be seen that the lateral acceleration in the simplified model

is equal to zero, while for the full model it is not. Another notable aspect is that the values of the roll angle and roll rate are also equal to zero, which was also anticipated since it was forced by the first simplification.

4

Spectral Analysis

In this chapter, the spectral analysis of the previously defined models is performed using different methods: an analytical method based on the state-space form, an experimental method utilising the periodograms extracted with the `fft.m` routine in `MATLAB`, and another experimental approach that applies a smoothing filter to the previously obtained periodograms.

The first method of calculation is the analytical method, which consists in using the following expression,

$$S_{\bar{y}\bar{y}}(\omega) = |H(\omega)|^2 S_{\bar{u}\bar{u}}(\omega). \tag{4.1}$$

In this case since the input used is a white noise with spectral density,

$$S_{\bar{u}\bar{u}} = 1, \tag{4.2}$$

the PSD of the outputs is obtained as,

$$S_{\bar{y}\bar{y}}(\omega) = |H(\omega)|^2. \tag{4.3}$$

To obtain this in `MATLAB`, the function bode is used between the input w_2 and each of the outputs, states and lateral acceleration, to obtain the magnitude of the transfer function. The result of each transfer function is later multiplied by itself to obtain each $S_{\bar{y}\bar{y}}(\omega)$. The resulting analytical PSDs are included in Figure 4.1 for both models.

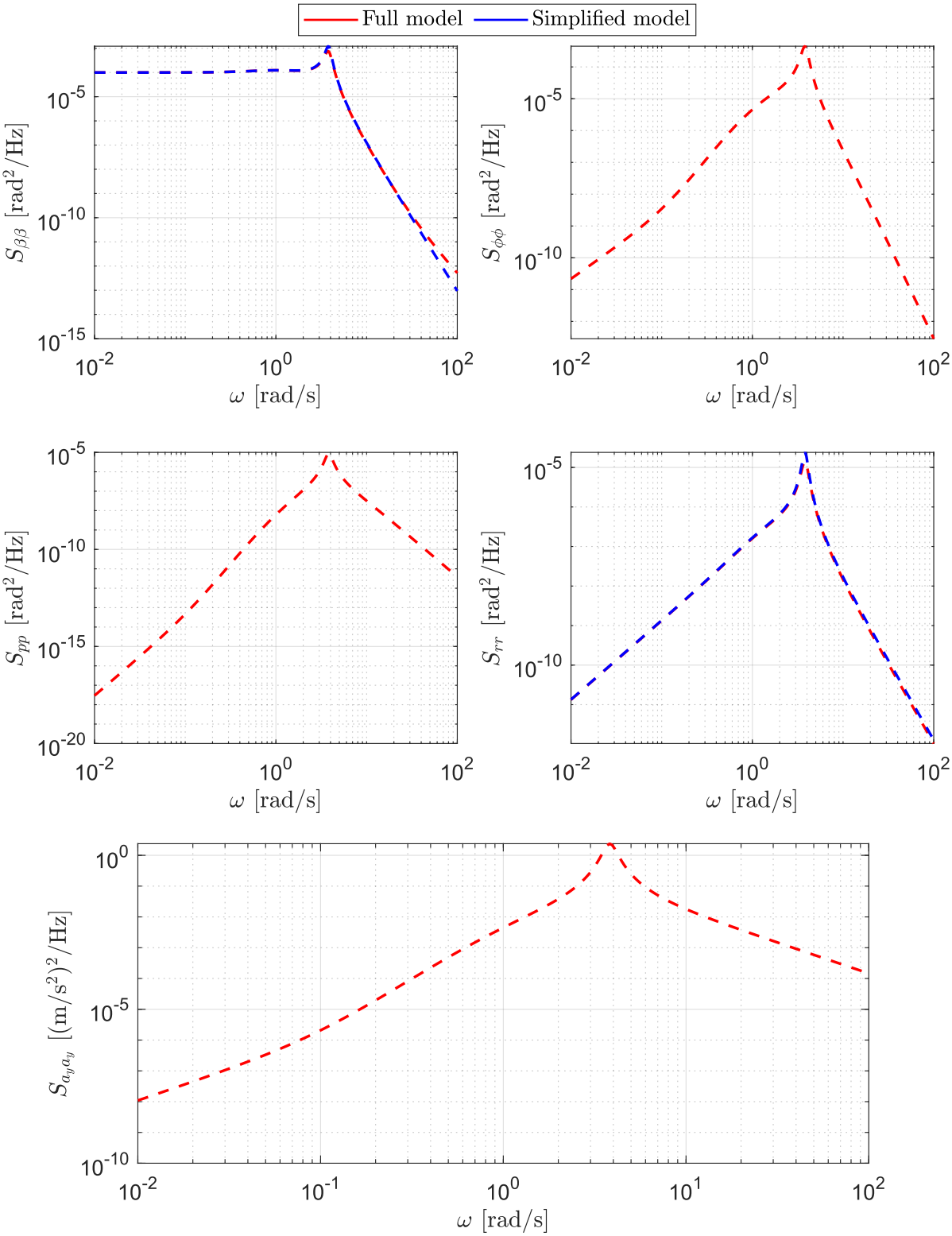

Figure 4.1: Representation of the analytical PSDs of the state variables and lateral acceleration a_y for both models considered.

From Figure 4.1 several key aspects can be observed. To start off, it can be seen how only two of the subplots show nonzero PSDs for the simplified model, the state β and the state r. Based on the construction of the simplified model, it makes sense that no PSDs appear for the roll angle and roll rate, since they are considered zero as a simplification. With respect to the lateral acceleration, the

reason why it does not show PSD is linked to the explanation given in the previous chapter. When considering a constant course, the equation Y remains in balance and the lateral acceleration is zero. When a signal is zero in all its domain, its PSD is also zero. This can be demonstrated as,

$$x(t) = 0 \Rightarrow R_{xx}(\tau) = \mathbb{E}\left[x(t)x(t+\tau)\right] = \mathbb{E}\left[0\right] = 0 \Rightarrow S_{xx}(\omega) = \int_{-\infty}^{\infty} R_{xx}(\tau)e^{-j\omega\tau}d\tau = 0. \tag{4.4}$$

Another important aspect to consider is the location and magnitude of the peaks in the Power Spectral Densities (PSDs). These peaks correspond to the excitation at the characteristic frequency of the dominant eigenmotions, which, in this case, is the Dutch Roll. This motion is associated with lateral turbulence, analogous to a rudder deflection. The specific locations of the peaks are provided in Table 4.1 for both the full and simplified models.

PSD	$\boldsymbol{\omega}$ [rad/s]	
	Full model	**Simplified model**
$S_{\beta\beta}$	3.8189	3.8189
$S_{\phi\phi}$	3.8189	-
S_{pp}	3.8189	-
S_{rr}	3.8189	3.8189
$S_{a_y a_y}$	3.8189	-

Table 4.1: Peak frequencies for the full model and simplified model PSDs.

A comparison of these results with the natural frequencies obtained in Table 2.3 and Table 2.4, for the complete model and the simplified model, respectively, further corroborates the previous explanation. The frequencies are nearly identical for both cases.

Regarding the peak values, they are associated with the amount of energy at each frequency, highlighting the dominant nature of the Dutch roll eigenmotion in comparison to the Spiral and Aperiodic roll. When comparing both models, the simplified model shows a higher peak, which can likely be attributed to a lower damping ratio. Revisiting Table 2.3 and Table 2.4 and comparing the damping ratios further supports this conclusion, confirming the consistency of the results with the figure. This reduction in the damping ratio is associated with the introduction of the roll-damper for the controlled full model.

The second method used for spectral analysis is based on estimating the periodograms, using the `fft.m` function incorporated in `MATLAB`. The first step in this method is to calculate the Discrete Fourier Transform (DFT) of each signal $X[K]$ using the Fast Fourier Transform (FFT) algorithm. Once the DFT is obtained, the next step is the extraction of the periodograms, which are computed using the expression from [3]:

$$\Phi[k] = \frac{1}{N}|X[k]|^2, \quad k = 1, 2, \ldots, N, \tag{4.5}$$

where the indices start at 1 to match the notation used in `MATLAB`. The calculated periodograms provide an initial estimate of the discrete PSD. However, this estimate differs from the continuous-time spectral density. Transforming a discrete version of a signal with time step Δt is equivalent to transforming the continuous signal, copying and shifting it, and then scaling it by $1/\Delta t$ [3]. To obtain the continuous-time spectral density, the periodogram must be scaled by Δt. Therefore, the final result is,

$$S_{xx}(\omega) = \Delta t \cdot \Phi[k]. \tag{4.6}$$

The resulting estimates of the PSDs are exposed in Figure 4.2 for the full model and in Figure 4.3 for the simplified model.

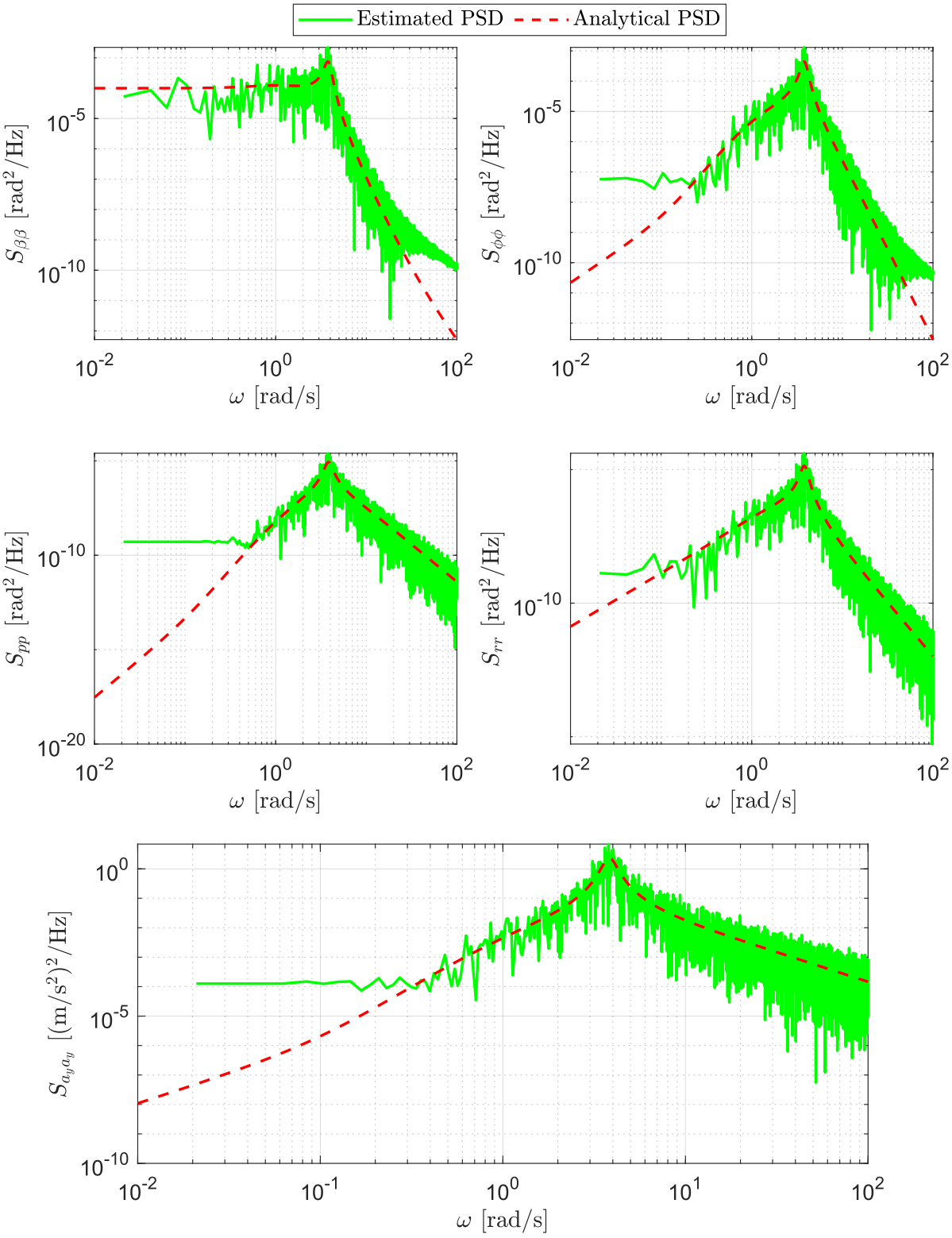

Figure 4.2: Representation of the estimated PSDs overlapped with the analytical PSDs of the state variables and lateral acceleration a_y for the full model.

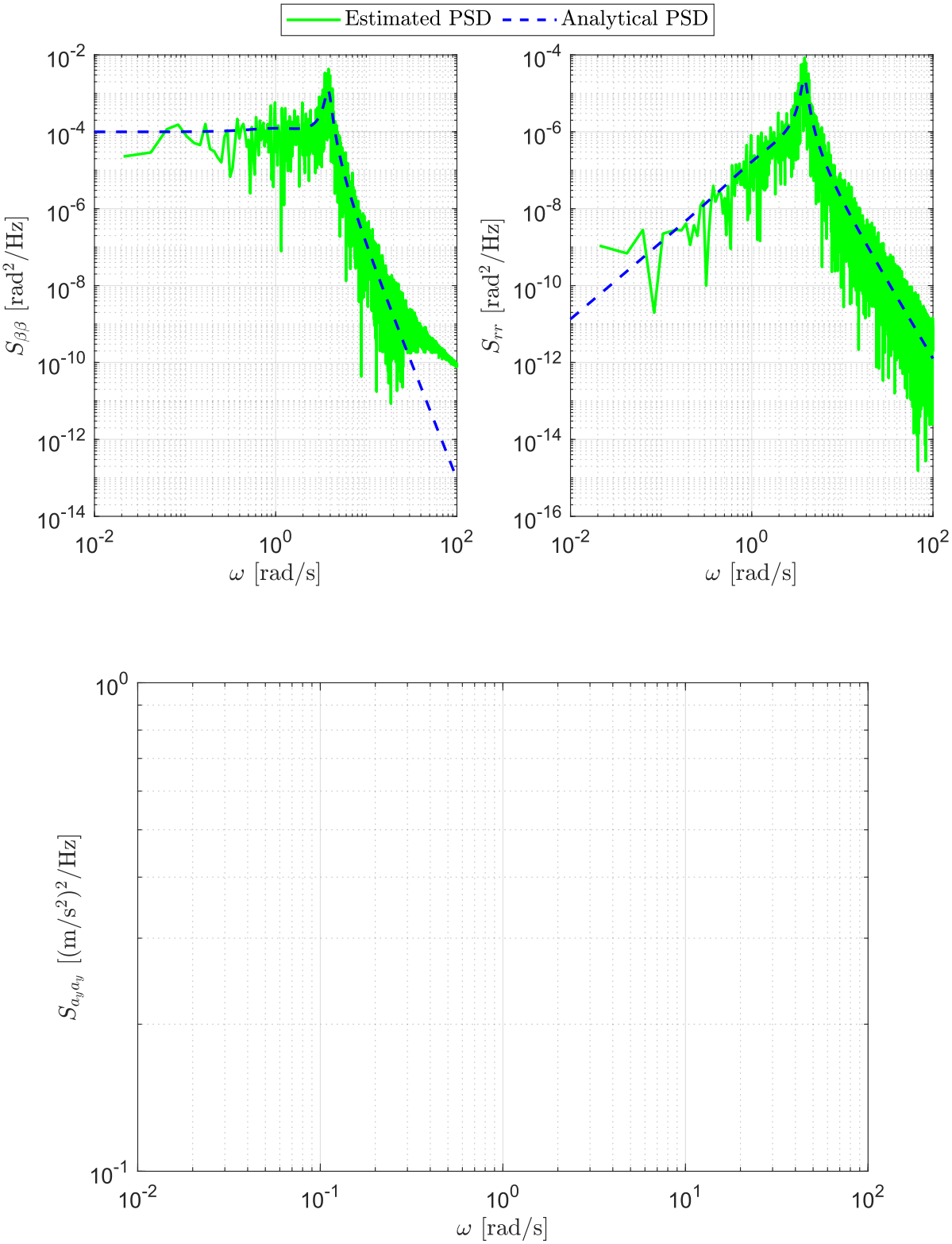

Figure 4.3: Representation of the estimated PSDs overlapped with the analytical PSDs of the state variables and lateral acceleration a_y for the simplified model.

From the figures, it is evident that contamination increases at each frequency, which is expected since the estimation is based on only one realisation of the time-domain simulations. However, the overall trend in both figures remains consistent with the analytical solution. In the case of the simplified model,

although the lateral acceleration was expected to be zero, the plot is still presented since it is an output of the system.

Finally, the last method for calculating the PSDs is applying a smoothing filter to the obtained periodograms, such that,

$$\Phi_{\text{estimate}}[k] = 0.25 \cdot \Phi[k-1] + 0.5 \cdot \Phi[k] + 0.25 \cdot \Phi[k+1]. \tag{4.7}$$

The results for the full and simplified model are included in Figure 4.4 and Figure 4.5 respectively.

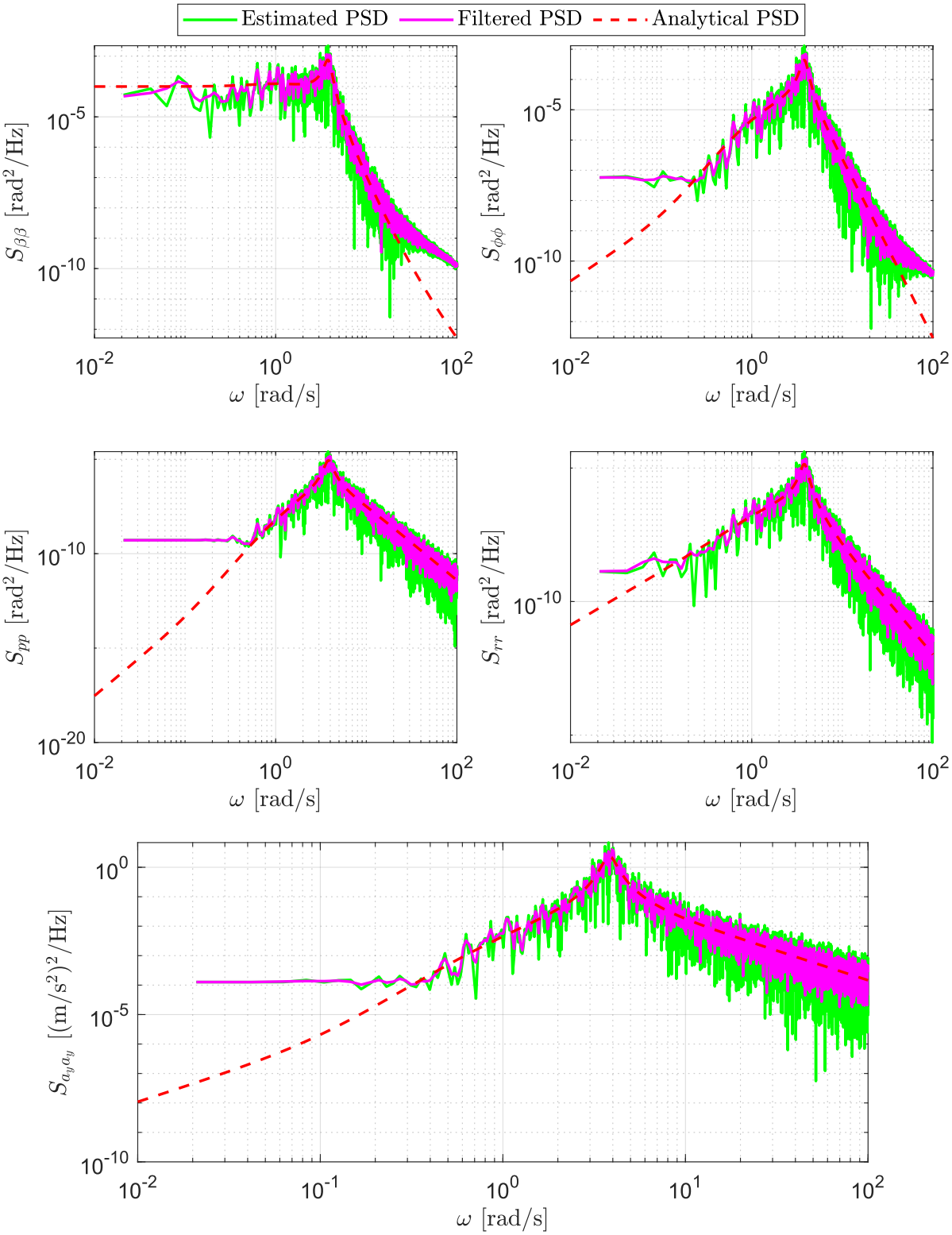

Figure 4.4: Representation of the filtered and unfiltered estimated PSDs overlapped with the analytical PSDs of the state variables and lateral acceleration a_y for the full model.

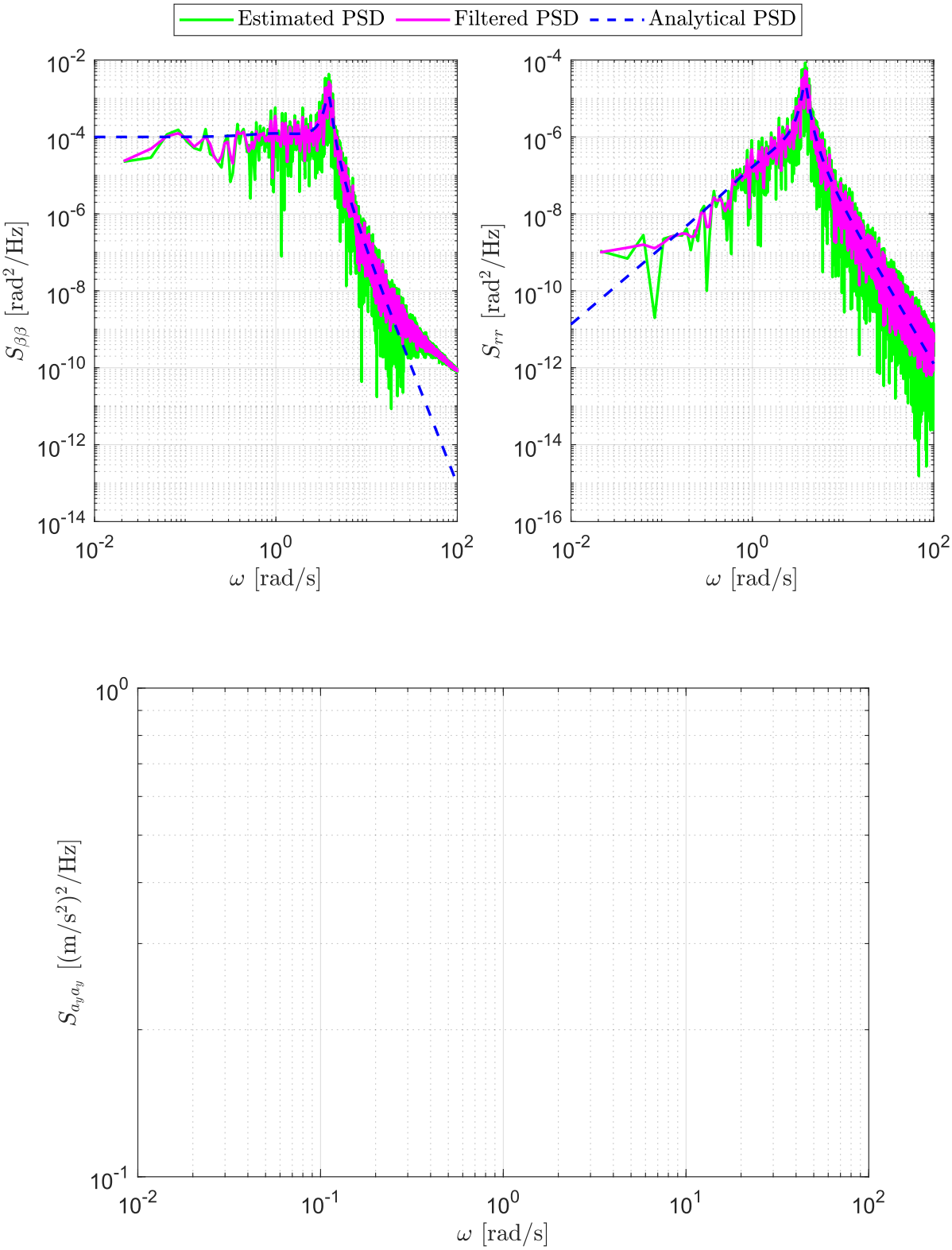

Figure 4.5: Representation of the filtered and unfiltered estimated PSDs overlapped with the analytical PSDs of the state variables and lateral acceleration a_y for the simplified model.

From the figures, a noticeable reduction in overall noise is observed in the estimated PSDs. The applied filter smooths the periodogram by averaging neighbouring values, effectively reducing variability and yielding a more stable estimate. In some cases, this results in a closer approximation to the analytical

solution. However, since the estimate is based on a single realisation, it remains sensitive to its inherent variability, highlighting the importance of using more than one measurement, i.e. ensemble averaging, for better accuracy.

5

Variance estimation

From the results obtained in the previous chapter, the variances have been computed for both models and for the different methods of calculating the PSDs. The general procedure for calculating the variance is by following the equation,

$$\sigma_y^2 = \frac{1}{\pi} \int_0^{+\infty} S_{yy}(\omega)\, \mathrm{d}\omega. \tag{5.1}$$

Since the obtained PSD results are discrete, the chosen approach for calculating the integrals in `MATLAB` is to compute the areas under the curves using the trapezoidal rule. A key aspect of variance calculation is its strong dependence on the number of signal measurements N or, for a fixed Δt, the measurement time T. Increasing this time enables a higher frequency resolution for the estimated PSDs, significantly impacting the results. Therefore, in this chapter, the measurement time has been increased from $T = 60s$ (as used in previous sections) to $T = 300s$. Taking all of the above into account, the calculated variances are presented in Table 5.1.

Model	$\sigma^2_{\boldsymbol{\beta}}$	$\sigma^2_{\boldsymbol{\phi}}$	$\sigma^2_{\frac{\mathbf{pb}}{\mathbf{2V}}}$	$\sigma^2_{\frac{\mathbf{rb}}{\mathbf{2V}}}$	$\sigma^2_{\mathbf{a_y}}$
			Analytical PSD		
Full Model	3.36208×10^{-4}	1.44779×10^{-4}	2.85618×10^{-6}	4.61448×10^{-6}	8.40895×10^{0}
Simplified	4.14515×10^{-4}	0.00	0.00	6.31599×10^{-6}	0.00
			Experimental PSD		
Full Model	3.47558×10^{-4}	1.49610×10^{-4}	2.93745×10^{-6}	4.76922×10^{-6}	8.67120×10^{0}
Simplified	4.45418×10^{-4}	0.00	0.00	7.23282×10^{-6}	0.00
			Filtered PSD		
Full Model	3.47514×10^{-4}	1.49610×10^{-4}	2.93745×10^{-6}	4.76922×10^{-6}	8.67120×10^{0}
Simplified	4.45399×10^{-4}	0.00	0.00	7.23282×10^{-6}	0.00
			Time Traces		
Full Model	3.47557×10^{-4}	1.49610×10^{-4}	2.93745×10^{-6}	4.76921×10^{-6}	8.67120×10^{0}
Simplified	4.45353×10^{-4}	0.00	0.00	7.23282×10^{-6}	0.00

Table 5.1: Variance results for a measurement time $T = 300s$ for different PSD computation methods on both models.

From the previous results, several conclusions can be drawn. First, it is evident that the variance results differ between the models for the same states. This result was expected, as previously discussed, since the models have slightly different PSD solutions. Specifically, the simplified model has a lower damping at the resonant frequency, leading to a higher PSD, which increases the area under the curve and, consequently, the variance values. Another aspect to mention is that since the roll angle and rate, as well as the lateral acceleration a_y, have zero PSD functions, their associated variances are also zero.

Another point to address is the comparison between the methods used to compute the PSDs. It is apparent that the variance values from the time-domain simulation-based PSD computations are very similar for each model. This makes sense as these methods are derived from the same signal, thus eliminating discrepancies caused by a lack of realisations; these discrepancies are the main source of the differences between the results obtained through these methods and the analytical solution. This phenomenon can be clearly demonstrated by running the same code multiple times, generating different random signals, and observing how the variance of the three estimated methods fluctuates. Despite these variations, all tests showed that the fluctuations remained within the same order of magnitude as the analytical solution, supporting the use of the periodogram as a first estimate of the true PSD.

6

Conclusion

This practical assignment has provided hands-on experience with analysing stochastic processes, specifically focussing on the response of a Cessna Ce500 Citation I subjected to asymmetrical atmospheric turbulence, modelled using the Dryden spectrum.

To begin, the first chapter covered the modelling of the specified aircraft, including the incorporation of the turbulence model under different flight assumptions: a full model and a simplified model without roll, maintaining a constant course. In addition, a stability analysis was conducted, which led to the design of a roll-damper to stabilise the entire model.

In the second chapter, time-domain simulations were performed based on the models defined earlier, demonstrating the relationship between lateral turbulence and the system states. The lateral acceleration in the simplified model was observed to always be zero for any lateral input, confirming the validity of the assumptions made during model design.

The third chapter focused on Power Spectral Density (PSD) computations for different models using three distinct methods. The results illustrated that PSD peaks correspond to dominant eigenmotions at specific frequencies. It was also shown that reduced damping in the simplified model led to higher peak values. Furthermore, the periodogram was validated as a reasonable initial PSD estimate, although it introduced excessive noise. The application of a smoothing filter significantly improved the results by averaging values and bringing the estimation closer to the analytical solution.

Finally, in the fourth chapter, variance calculations were performed, revealing how variance differs between models due to variations in their PSD solutions. The simplified model exhibited higher variance due to lower resonance damping. A comparison of PSD computation methods showed that time-domain simulations provided consistent variance values across models since they originated from the same signal, reducing inconsistencies. Although some fluctuations occurred due to the randomness of signal generation, they remained within the same order of magnitude as the analytical solution.

In general, this study validated the modelling approach and analysis methods, demonstrating their reliability in assessing stochastic responses in aircraft dynamics.

References

[1] J.A. Mulder & W.H.J.J. van Staveren & J.C. van der Vaart & E. de Weerdt & C.C. de Visser A.C. int Veld & E. Mooij. *Flight Dynamics. Lecture Notes AE3302.* Delft University of Technology, 2013.

[2] U.S. Department of Defense. *Flying Qualities of Piloted Airplanes (MIL-F-8785C).* Tech. rep. U.S. Department of Defense, 1980. URL: `http://www.everyspec.com`.

[3] J.A. Mulder & J.C. van der Vaart & W.H.J.J. van Staveren & Q.P. Chu & M. Mulder. *Aircraft Responses to Atmospheric Turbulence.* Delft University of Technology, 2020.

A

Tables

Definition
$\mu_b = \frac{m}{\rho S_b}$
$K_X^2 = \frac{I_{xx}}{mb^2}$
$K_Z^2 = \frac{I_{zz}}{mb^2}$
$J_{XZ} = \frac{I_{xz}}{mb^2}$

Table A.1: Moments and products of inertia of the asymmetric motions.

	$y\ldots$	$l\ldots$	$n\ldots$
β	$\frac{VC_{Y_\beta}}{2b\mu_b}$	$\frac{VC_{l_\beta}K_Z^2+C_{n_\beta}K_{XZ}}{4b\mu_b(K_X^2K_Z^2-K_{XZ}^2)}$	$\frac{VC_{l_\beta}K_{XZ}+C_{n_\beta}K_X^2}{4b\mu_b(K_X^2K_Z^2-K_{XZ}^2)}$
φ	$\frac{VC_L}{2b\mu_b}$	0	0
p	$\frac{VC_{Y_p}}{2b\mu_b}$	$\frac{VC_{l_p}K_Z^2+C_{n_p}K_{XZ}}{4b\mu_b(K_X^2K_Z^2-K_{XZ}^2)}$	$\frac{VC_{l_p}K_{XZ}+C_{n_p}K_X^2}{4b\mu_b(K_X^2K_Z^2-K_{XZ}^2)}$
r	$\frac{VC_{Y_r}-4\mu_b}{2b\mu_b}$	$\frac{VC_{l_r}K_Z^2+C_{n_r}K_{XZ}}{4b\mu_b(K_X^2K_Z^2-K_{XZ}^2)}$	$\frac{VC_{l_r}K_{XZ}+C_{n_r}K_X^2}{4b\mu_b(K_X^2K_Z^2-K_{XZ}^2)}$
δ_a	$\frac{VC_{Y_{\delta_a}}}{2b\mu_b}$	$\frac{VC_{l_{\delta_a}}K_Z^2+C_{n_{\delta_a}}K_{XZ}}{4b\mu_b(K_X^2K_Z^2-K_{XZ}^2)}$	$\frac{VC_{l_{\delta_a}}K_{XZ}+C_{n_{\delta_a}}K_X^2}{4b\mu_b(K_X^2K_Z^2-K_{XZ}^2)}$
δ_r	$\frac{VC_{Y_{\delta_r}}}{2b\mu_b}$	$\frac{VC_{l_{\delta_r}}K_Z^2+C_{n_{\delta_r}}K_{XZ}}{4b\mu_b(K_X^2K_Z^2-K_{XZ}^2)}$	$\frac{VC_{l_{\delta_r}}K_{XZ}+C_{n_{\delta_r}}K_X^2}{4b\mu_b(K_X^2K_Z^2-K_{XZ}^2)}$
β_g	$\frac{VC_{Y_\beta}}{2b\mu_b}$	$\frac{VC_{l_\beta}K_Z^2+C_{n_\beta}K_{XZ}}{4b\mu_b(K_X^2K_Z^2-K_{XZ}^2)}$	$\frac{VC_{l_\beta}K_{XZ}+C_{n_\beta}K_X^2}{4b\mu_b(K_X^2K_Z^2-K_{XZ}^2)}$

Table A.2: Symbols appearing in the general state-space representation.

Level	**Category**	**Class**	**min** ζ_d	**min** $\zeta_d\omega_{n_d}$	**min** ω_{n_d}
Level 1	A(C, GA)	IV	0.4		1.0
	A	I and IV	0.19	0.35	1.0
		II and III	0.19	0.35	0.4
	B	all	0.08	0.15	0.4
	C	I, II-C, IV	0.08	0.15	1.0
		II-L, III	0.08	0.10	0.4
Level 2	all	all	0.02	0.05	0.4
Level 3	all	all	0		0.4

Table A.3: Minimum Dutch Roll frequency and damping [2].